Protein Science (1998), 7:2550–2559. Cambridge University Press. Printed in the USA.

Dominant role of local dipolar interactions in phosphate binding to a receptor cleft with an electronegative charge surface: Equilibrium, kinetic, and crystallographic studies

POLLY S. LEDVINA,[1] AH-LIM TSAI,[2] ZHONGMIN WANG,[3,4] EDWARD KOEHL,[1] AND FLORANTE A. QUIOCHO[1,3,4]

[1]Howard Hughes Medical Institute, Baylor College of Medicine, Houston, Texas 77030
[2]Division of Hematology, Internal Medicine, University of Texas Health Science Center, Houston, Texas 77030
[3]Graduate Program in Structural and Computational Biology and Molecular Biophysics, Baylor College of Medicine, Houston, Texas 77030
[4]Verna and Marrs McLean Department of Biochemistry, Baylor College of Medicine, Houston, Texas 77030

(RECEIVED June 5, 1998; ACCEPTED August 24, 1998)

Abstract

Stringent specificity and complementarity between the receptor, a periplasmic phosphate-binding protein (PBP) with a two-domain structure, and the completely buried and dehydrated phosphate are achieved by hydrogen bonding or dipolar interactions. We recently found that the surface charge potential of the cleft between the two domains that contains the anion binding site is intensely electronegative. This novel finding prompted the study reported here of the effect of ionic strength on the equilibrium and rapid kinetics of phosphate binding. To facilitate this study, Ala197, located on the edge of the cleft, was replaced by a Trp residue (A197W PBP) to generate a fluorescence reporter group. The A197W PBP–phosphate complex retains wild-type K_d and X-ray structure beyond the replacement residue. The K_d (0.18 μM) at no salt is increased by 20-fold at greater than 0.30 M NaCl. Stopped-flow fluorescence kinetic studies indicate a two-step binding process: (1) The phosphate (L) binds, at near diffusion-controlled rate, to the open cleft form (P_o) of PBP to produce an intermediate, P_oL. This rate decreases with increasing ionic strength. (2) The intermediate isomerizes to the closed-conformation form, P_cL. The results indicate that the high specificity, affinity, and rate of phosphate binding are not influenced by the noncomplementary electronegative surface potential of the cleft. That binding depends almost entirely on local dipolar interactions with the receptor has important ramification in electrostatic interactions in protein structures and in ligand recognition.

Keywords: anion binding sites; electrostatic interaction; fast kinetics; hinge-bending motion; noncomplementary surface charge sites; phosphate-binding protein; X-ray structure

The phosphate-binding protein (PBP) is an excellent and well-defined system to study electrostatic interactions, especially in relation to charged ligand binding. PBP is a member of a very large protein family that serves as primary receptors of active transport for a wide variety of ligands in bacterial cells. Our extensive crystallographic analysis, including recent ultra-high resolution (0.98 and 1.05 Å) structures of the PBP–phosphate complex, and site-directed mutagenesis and equilibrium ligand-binding studies have revealed several novel features of the PBP–phosphate interaction (Luecke & Quiocho, 1990; Wang et al., 1994, 1997; Ledvina et al., 1996; Yao et al., 1996). (1) The bound phosphate is completely dehydrated and totally engulfed within a cleft between two domains. Access to and from the cleft is accompanied by a hinge-bending between the two domains. (2) The phosphate is held in place by 12 hydrogen bonds (11 with donor groups and one with a carboxylate acceptor group), as well as one salt link to an Arg that is in turn salt linked to an Asp. (3) The charge of the buried phosphate is stabilized mainly by local dipoles surrounding the ligand, including those making hydrogen bonds to the phosphate. Although helix N-termini are close to the phosphate, helix macrodipoles play no role in this process (see also Quiocho et al., 1987; Åqvist et al., 1991; He & Quiocho, 1993). (4) The hydrogen bond between an Asp carboxylate oxygen and a phosphate oxygen, which is extremely short (2.432 Å distance) as established in the ultra-high resolution structures, confers the exquisite specificity of the PBP and the phosphate transport system. Although the distance is within the proposed range of low barrier hydrogen bonds with

Reprint requests to: Florante A. Quiocho, HHMI/Baylor College of Medicine, 1 Baylor Plaza, Houston, Texas 77030; e-mail: faq@dino.bcm.tmc.edu.

Abbreviations: A197W PBP, a PBP with Ala197 replaced by a Trp; MDCC, N-[2-(1-maleimidyl)ethyl]-7-(diethylamino) coumarin-3-carboxamide; PBP, phosphate-binding protein; Pi, inorganic phosphate.

estimated energies of 12–24 kcal/mol (Hibbert & Emsley, 1990; Cleland & Kreevoy, 1994), the contribution of the short hydrogen bond to the phosphate binding affinity is no better than that of a normal hydrogen bond. (5) The surface electrostatic potential of the cleft that contains the binding site has been calculated to be predominantly electronegative.

Ligand-binding kinetic studies are necessary to more directly ascertain the influence of several factors that may affect association between phosphate and PBP, including electrostatic effects and hinge-bending motion. We have previously used stopped-flow fluorescence to obtain kinetic data for several periplasmic binding proteins (Miller et al., 1980, 1983; Vermersch et al., 1990; Jacobson et al., 1992). This has been possible because these proteins, as revealed by X-ray structure analysis, each contains one or more Trp residue in the binding site that can function as a natural ligand-sensitive fluorophore. Unfortunately, wild-type PBP does not contain a Trp residue in or near the binding site that is titratable by phosphate.

Brune et al. (1994) introduced a Cys residue (A197C) in one domain and on the edge of the binding site cleft of PBP and chemically attached a large synthetic fluorophore, N-[2-(1-maleimidyl)ethyl]-7-(diethylamino)coumarin-3-carboxamide (MDCC). This synthetic derivative of PBP was then used successfully as a phosphate-sensitive reporter molecule in stopped flow with actomyosin subfragment 1 ATPase.

To further extend our study on electrostatic interactions between PBP and phosphate, we choose to use a protein molecule with a more native-like structure that was also verifiable by X-ray crystallography. For this purpose Ala197 of PBP was mutated to Trp (A197W PBP). This mutant exhibits a quench in fluorescence upon phosphate binding that we have used to obtain stopped-flow kinetics and equilibrium ligand binding data and to investigate the effects of ionic strength on these data. The A197W PBP has wild-type phosphate binding affinity and has been verified by X-ray crystallography to retain native structure beyond the site of the mutation.

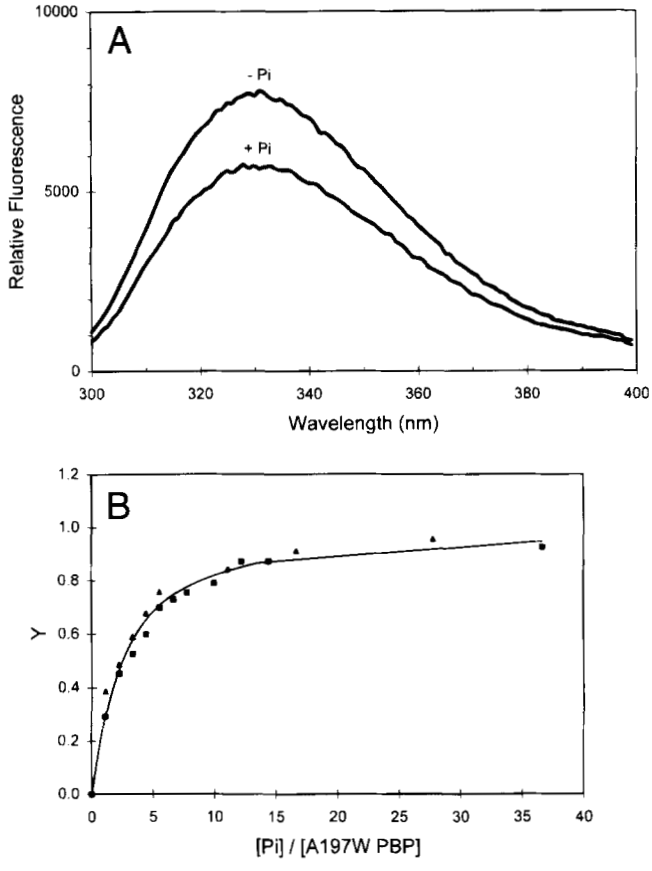

Fig. 1. Fluorescence spectra and Pi titration of A197W PBP. **A:** Fluorescence emission spectra of the A197W PBP (1 μM) in the absence and presence of saturating Pi (10 μM). Excitation wavelength was at 285 nm. The buffer was 50 mM Tris-acetate, pH 8.5. **B:** Fluorescence titration of the A197W PBP with Pi at 20 °C. The fluorescence decrease at 330 nm was titrated by the addition of microliter aliquots of Pi (0.10 mM) to 2 mL of protein (0.09 μM). The data, shown for two separate titrations, fit a simple binding model (Miller et al., 1983). The best fit K_d values determined for titration 1 and titration 2 were 0.20 and 0.16 μM, respectively. The smooth line represents the best fit of the two data for a second order binding process with K_d = 0.18 μM.

Results

A197W PBP and fluorescence quenching by phosphate binding

High yields of soluble A197W PBP were easily purified from the periplasm of BL21(D3) harboring pET-PBP197W. The fluorescence emission maximum of the A197W PBP is at 325 nM with 25% quenching, without shifting the emission maximum, occurring in the presence of excess Pi for the conditions described in Figure 1A. These results are in contrast to those obtained using MDCC-labeled PBP, where a very large increase in fluorescence is obtained upon phosphate binding (Brune et al., 1994).

Equilibrium ligand binding

As determined by the resin assay, the Pi binding activity of the A197W PBP appears to be that of the wild-type protein. At pH 8.5 under conditions of low ionic strength, the A197W PBP binds Pi with a K_d of 0.49 μM (Table 1), very close to that of the wild type (0.31 μM; Wang et al., 1997). This result is similar to that of Brune et al. (1994), where only a twofold reduction in affinity occurred with the attachment of the much bulkier synthetic fluorophore, MDCC, at residue 197.

The fluorescence decrease at 330 nm was used to monitor Pi binding of the A197W PBP in equilibrium titration experiments (Fig. 1B). The K_d (0.18 μM) determined for the mutant is about twofold smaller, but still in reasonable agreement with the value obtained by the resin assay. Brune et al. (1994) similarly reported smaller K_d values of PBP labeled with MDCC measured by fluorescence titration than by resin assay.

It has been shown, by the resin assay, that the binding affinity of Pi by wild-type PBP decreases with increasing ionic strength of the buffer (Wang et al., 1994). The limitations of determinations by the resin method, however, are decreased reliability for larger K_d values and the inherent sensitivity of the assay to salt conditions. Fluorescence titrations are more reliable for measuring weaker affinities (Miller et al., 1983; Vermersch et al., 1990) and, unlike the resin method, they are not inherently sensitive to ionic strength conditions.

The effect of salt (0–900 mM NaCl) on Pi binding to A197W PBP was measured by fluorescence titrations. Scatchard plots from these titrations, shown in Figure 2, demonstrate decreased Pi af-

Table 1. *Equilibrium dissociation constants of the A197W PBP-Pi complex*

Method	NaCl (M)	$K_d \times 10^6$ (M)
Resin assay[a]	0	0.49 (0.02)
Fluorescence titration[b]	0	0.18
	0.02	0.29
	0.05	0.76
	0.10	1.03
	0.30	3.36
	0.60	3.62
	0.90	3.74

[a]Resin assays were conducted at room temperature in 50 mM Tris-acetate, pH 8.5. Standard deviations, determined from triplicate assays, are given in parenthesis.

[b]Fluorescence titrations were conducted at 20 °C in 50 mM Tris-acetate, pH 8.5, and 0 to 900 mM NaCl. Deviation, determined from duplicate assays, is less than 15%.

finity in the presence of salt. About a 20-fold reduction in binding occurs at salt concentrations greater than 300 mM NaCl (Table 1).

Ligand-binding kinetics

The kinetics of Pi binding to the A197W PBP were measured in a rapid mixing, stopped-flow apparatus. Pi binding was followed as a decrease in fluorescence intensity at wavelengths greater than 325 nm (for examples, see Fig. 3). Only baseline fluorescence was observed when the protein was mixed with buffer alone. Time courses were fit to single exponential functions (data not shown) indicating only one event is being monitored by the fluorescent quenching.

The observed rate constants, k_{obs}, for the A197W PBP over a range of Pi and NaCl concentrations are shown graphically in Figure 4. The rates increase with increasing [Pi]. The effect of salt was to lower the observed rates. At faster rates (i.e., higher Pi and lower salt concentrations), greater portions of the binding reaction occur in the dead time of the apparatus. Therefore, with high salt (300–900 mM), it was possible to measure association rates over a range of 1–200 μM Pi, but in the absence or low concentration of salt, binding was too fast to measure at [Pi] > 8 μM.

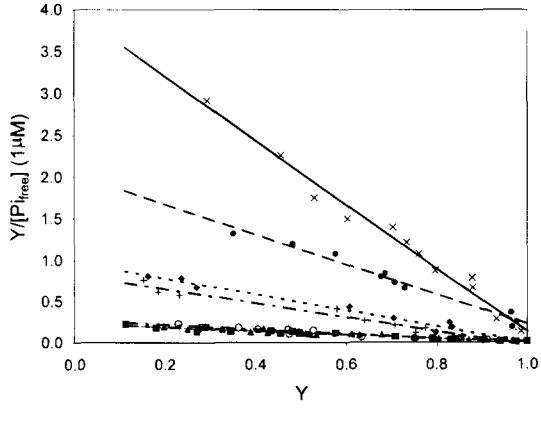

Fig. 2. Scatchard plots of Pi binding to A197W PBP in the presence of salt. Fluorescence titrations were conducted at 20 °C in 50 mM Tris-acetate, pH 8.5, and 0–900 mM NaCl (×, no salt; filled circle, 20 mM; filled diamond, 50 mM; +, 100 mM; open circle, 300 mM; filled up triangle, 600 mM; filled square, 900 mM). Protein concentrations were 0.09 μM for the titration without salt and 0.9–1.1 μM for those with salt. The lines show the best fit with K_d values shown in Table 1.

There is a linear dependence of k_{obs} on [Pi] only at the lower ranges of concentration (Fig. 4). In the experiments with high salt (>300 mM) and high [Pi] (>100 μM), a saturation of rates can be seen around 300 s^{-1}. Under conditions of low ionic strength, it was not possible to extend the phosphate range far enough to observe saturation with the A197W PBP; however, it has been observed under these conditions with the MDCC-labeled PBP (Brune et al., 1994).

The hyperbolic saturation phenomenon of k_{obs} vs. [Pi] indicates a two-step ligand binding process. The single-exponential kinetics of the fluorescence change suggest further that we are measuring the slow conformational change of the protein (not the initial phosphate-binding step to an open, unliganded protein, P_o) and that there is a rapid equilibrium process occurring before the final conformational change. These features are consistent with the following two-step Pi binding:

$$P_o + L \underset{k_{-1}}{\overset{k_1}{\rightleftarrows}} P_oL \overset{\text{slow}}{\underset{k_{-2}}{\overset{k_2}{\rightleftarrows}}} P_cL \qquad \text{(Scheme 1)}$$

where L represents the ligand, P_o and P_c the open and closed cleft forms, respectively, of the protein and

$$k_{obs} = k_2 * [L]/([L] + K_1) + k_{-2} \qquad (1)$$

$$K_1 = k_{-1}/k_1 \qquad (2)$$

$$K_2 = k_{-2}/k_2. \qquad (3)$$

This ligand-binding model was also proposed for L-arabinose-binding protein, another member of the transport receptor family (Vermersch et al., 1990). In the case of the arabinose-binding protein, however, the conformational change was fast relative to the actual binding process. Within the limits of the stopped-flow apparatus, the observed rates were linearly dependent on sugar, at all concentrations. The arabinose-binding protein data, therefore, could be described by a one-step binding mechanism with

$$k_{obs} = k_1 * [L] + k_{-1}. \qquad (4)$$

Equation 1 is similar to that of the one-step binding mechanism except that $[L]$ in Equation 4 is replaced by the effective concentration of P_oL after the first fast equilibrium is established. It is clear in the case of PBP that the Y-axis intercept of the plot, k_{obs} vs. [Pi] (Fig. 4), gives the value of k_{-2} (not k_{-1}), and when rates are measured at [Pi] much greater than K_1, k_{obs} plateaus to the value of $k_2 + k_{-2}$. Thus, k_{-2} and K_2 can be calculated and K_1 can be estimated from the initial slope of the curve (i.e., when [Pi] $\rightarrow 0$, k_2/K_1 will be the slope). This approach leads to k_{-2} values (60 to 150 s^{-1}) with most extreme deviations occurring at low salt concentrations (0–50 mM). In the low salt range, the high observed rates (>200 s^{-1}) decrease the reliability of the estimated rate constant. No dependence on salt (0–900 mM) is evident for k_2. To

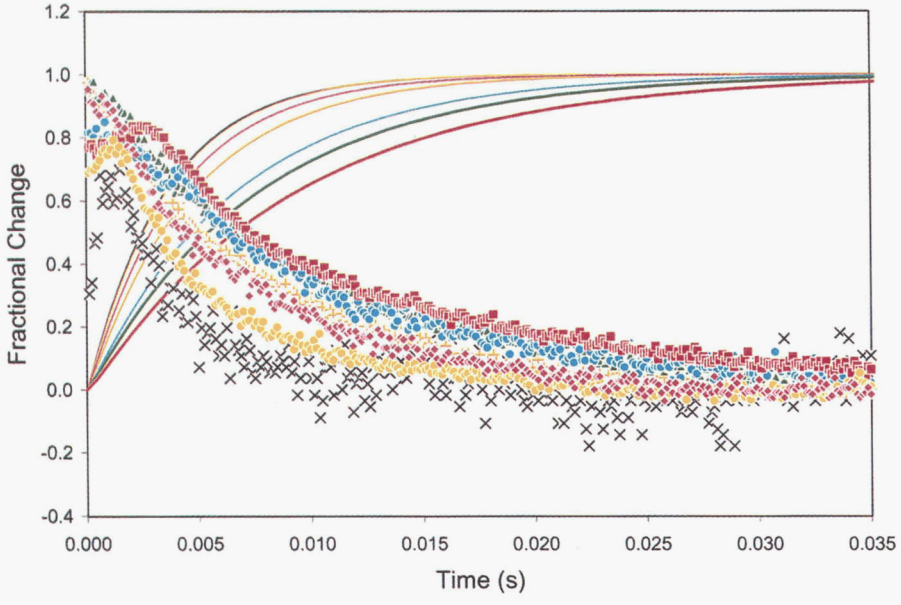

Fig. 3. Reaction between 1 μM A197W PBP and 8 μM Pi in the absence or presence of 20, 50, 100, 300, 600, and 900 mM NaCl. The fluorescence data (expressed as a normalized fractional change in fluorescence) for the binding experiments are shown (data points) for different salt concentrations (black ×, no salt; yellow filled circle, 20 mM; magenta filled diamond, 50 mM; orange +, 100 mM; blue open circle, 300 mM; green filled up triangle, 600 mM; red filled square, 900 mM). Each kinetic data set is the average of 5–10 repeats. Simulations of the normalized fractional change of $[P_cL]$ vs. time are also shown (theoretical curves) for different salt concentrations (black, no salt; yellow, 20 mM; magenta, 50 mM; orange, 100 mM; blue, 300 mM; green, 600 mM; and red, 900 mM). The parameters used to simulate each curve are as shown in Table 3.

obtain more reliable k_2 and k_{-2} values, a three parameter nonlinear regression was performed with Equation 1 for each salt concentration (100–900 mM). Using the averaged values of k_2 (289 ± 53 s^{-1}) and k_{-2} (59 ± 27 s^{-1}) thus obtained, a second cycle of one-parameter nonlinear regression was undertaken in order to obtain K_1 values. This second cycle yielded fits that match quite well the observed hyperbolic rates as a function of [Pi] at all salt conditions (Fig. 4), and K_1 values that are salt concentration dependent (Table 2). Moreover, the calculated values of $K_1 * K_2$ by this method (Table 2) are in reasonable agreement with the experimentally determined K_{eq} (Table 1).

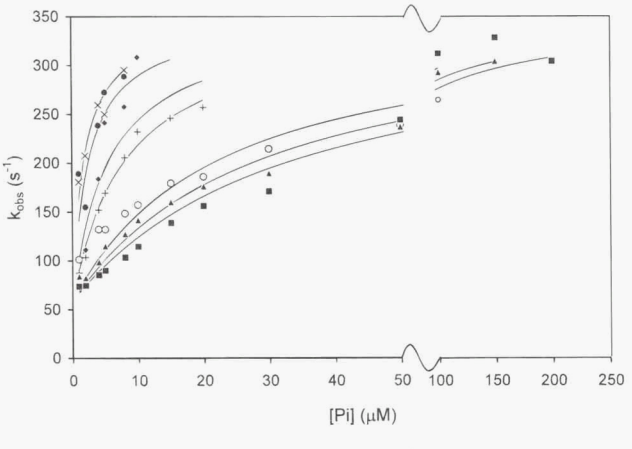

Fig. 4. Rate constant, k_{obs}, as a function of [Pi] at different salt concentrations (×, no salt; filled circle, 20 mM; filled diamond, 50 mM; +, 100 mM; open circle, 300 mM; filled up triangle, 600 mM; filled square, 900 mM). The lines show fitting of the data to Equation 1 that governs Scheme 1 (see text).

It was necessary to conduct simulations of Pi binding to obtain k_1 and k_{-1} for the first binding step as a function of salt concentrations. Optimal simulations, using the program SCoP, were conducted with the following conditions: The k_{-1} and k_1 were varied while keeping the k_{-1}/k_1 ratio equal to K_1 (Table 2). The value of k_2 was fixed at 289 s^{-1}, and k_{-2} was varied within the range of the standard deviation to give the final values shown in Table 2. (Varying k_2 or both k_2 and k_{-2} within the range of the standard deviation gave very similar results. Optimal simulation could not be achieved by keeping both k_2 and k_{-2} fixed.) To obtain a converged set of k_1 and k_{-1} values, the degrees of freedom of the numerical integration were further reduced by maintaining relatively constant values of k_{-1} in the simulations of the data at all Pi and salt concentrations. The values of k_1 and k_{-1} produced from the optimal simulation conditions are summarized in Table 2. The values of k_{-1} and k_{-2} are nearly constant, whereas those of k_1 decrease with increasing salt concentrations. The values of k_1 and k_{-1}, especially in the absence of salt, indicate Pi binding close to diffusion-controlled rate.

A plot of the normalized fractional change of $[P_cL]$ is useful in revealing the difference in rates (for examples, see Fig. 3). The normalized P_cL obtained from the simulation appears to closely match the observed fractional change of P_cL. Moreover, the simulation results also predicted the observed amplitude of P_cL very nicely (not shown).

We can conclude that the mechanism of Pi binding to PBP is a two-step equilibrium binding mechanism (Scheme 1), and the Trp fluorescence change is reporting step 2, the conformational change

Table 2. *Constants of the reaction between A197W PBP and phosphate*

	[NaCl] (M)						
Constant	0	0.02	0.05	0.1	0.3	0.6	0.9
k_{-2} (s^{-1})	77.2	77.8	73.7	71.1	74.9	69.8	62.5
k_2 (s^{-1})	289	289	289	289	289	289	289
$K_1 \times 10^6$ (M)	1.8	2.6	5.6	7.9	22.6	28.9	34.3
K_2	0.27	0.27	0.26	0.25	0.26	0.24	0.22
$K_1 * K_2 \times 10^6$ (M)	0.49	0.70	1.46	1.98	5.88	6.94	7.55
$k_1 \times 10^{-8}$ (M^{-1} s^{-1})	25.0	15.6	7.8	5.4	2.6	2.1	1.3
k_{-1} (s^{-1})	4,525	3,978	4,418	4,263	5,589	6,077	4,454

in going from the ligand-bound open form, P_oL, to the ligand-bound closed form, P_cL. As has been previously shown, Scheme 1 can be expanded to include an equilibrium step of isomerization between the unliganded forms, P_c and P_o, that precedes the initial ligand binding to P_o (Vermersch et al., 1990; Walmsley et al., 1992). A slow isomerization step between unliganded forms has been indicated in the kinetic studies of the periplasmic C4-dicarboxylate binding protein (DctP), where observed association rates are inversely proportional to ligand concentration (Walmsley et al., 1992). Our results for the A197W PBP (Fig. 4) differ sharply from those of DctP, providing evidence that the observed slow isomerization is indeed occurring between the two ligand-bound forms, and not between unliganded forms. For PBP, as for many other amino acid and sugar binding proteins studied in our laboratory (Miller et al., 1983; Vermersch et al., 1990), the initial equilibrium between P_o and P_c must lie predominantly toward P_o.

Structure of the closed cleft A197W PBP with bound phosphate

The closed structure of the A197W PBP mutant with bound Pi was determined by direct phasing with the wild-type structure and refined against the 1.7 Å resolution data to an *R*-factor of 0.205 and *R*-free of 0.269 and good geometry (Table 3). Comparison with the wild-type structure refined at a comparable resolution of 1.66 Å (Table 3; see also Wang et al., 1994; Yao et al., 1996), shows that the Trp197 mutation has essentially no effect on the overall tertiary structure. When overlapped with the wild-type structure (Fig. 5A), there is an overall α-carbons RMS deviation (RMSD) of 0.25 Å and no differences in the Pi binding site. The single A197W mutation, located in Domain II,[5] is on the edge of the cleft, close to the protein surface and far from the phosphate-binding site (Fig. 5A). The distance between the Pi and the closest atom of Trp197 is about 12 Å, with all intervening residues in the wild-type conformation. Moreover, the hydrogen-bonding interactions between the Pi and the mutant protein are indistinguishable from those of the wild-type complex (Fig. 6).

The large side chain of the Trp substitution produced only very minor local conformational changes relative to the wild-type structure (Fig. 5B). The side chains of two residues around the mutation site, Gln201 and Leu291, have moved slightly to accommodate the larger Trp side chain. No new interactions are formed between the mutated residue and the rest of the protein. The three main chain

Table 3. *Diffraction data and refinement statistics for the ligand-bound closed structures of the wild-type and A197W PBPs*

Parameter	Native PBP[a]	A197W PBP
Data collection		
Resolution range (Å)	20–1.66	15–1.7
Unique reflections (no sigma cutoff)[b]	36,946	35,260
R_{sym}	0.056	0.086
Completeness (%)	92.1	92.3
Space group	$P2_12_12_1$	$P2_12_12_1$
Unit cell (Å)	a = 41.97	a = 41.41
	b = 63.98	b = 62.76
	c = 123.97	c = 122.73
Refinement		
R-factor	0.205	0.203
R-free	0.263	0.269
Resolution (Å)	20.0–1.66	15–1.7
Highest resolution shell (Å)	1.74–1.66	1.78–1.70
Completeness (%)	54.9	63.6
RMSD		
Bond distance (Å)	0.013	0.013
Bond angle (°)	1.554	1.661
Dihedrals (°)	23.964	23.788
Impropers (°)	1.447	1.552
Number of atoms		
Protein	2,438	2,447
Ligand	5	5
Water	189	411

[5]The two domains of PBP are identified as Domains I and II, which correspond to the N- and C-domains, respectively, that were initially adapted and previously used extensively (Quiocho et al., 1977; Quiocho, 1991). This modification of nomenclature has been necessitated by the fact that, although all structures of binding proteins (at least a dozen) determined thus far consist of two domains, about half (PBP included; Fig. 6) have both the N- and C-terminal ends confined to one domain, Domain I (Kang et al., 1991; Yao et al., 1994; Nickitenko et al., 1995).

[a]The structure previously refined at 1.7 Å (Wang et al., 1994; Yao et al., 1996) has been further refined, using XPLOR, to include reflections to 1.66 Å and to obtain the value of *R*-free with 10% of the data randomly removed. Although the structure of native PBP-phosphate complex has been refined at ultra high resolution (about 1 Å resolution) (Wang et al., 1997), we preferred to compare the structures of the complexes with the native and A197W PBPs at comparable resolutions.

[b]These total unique reflections were used in both structure refinements.

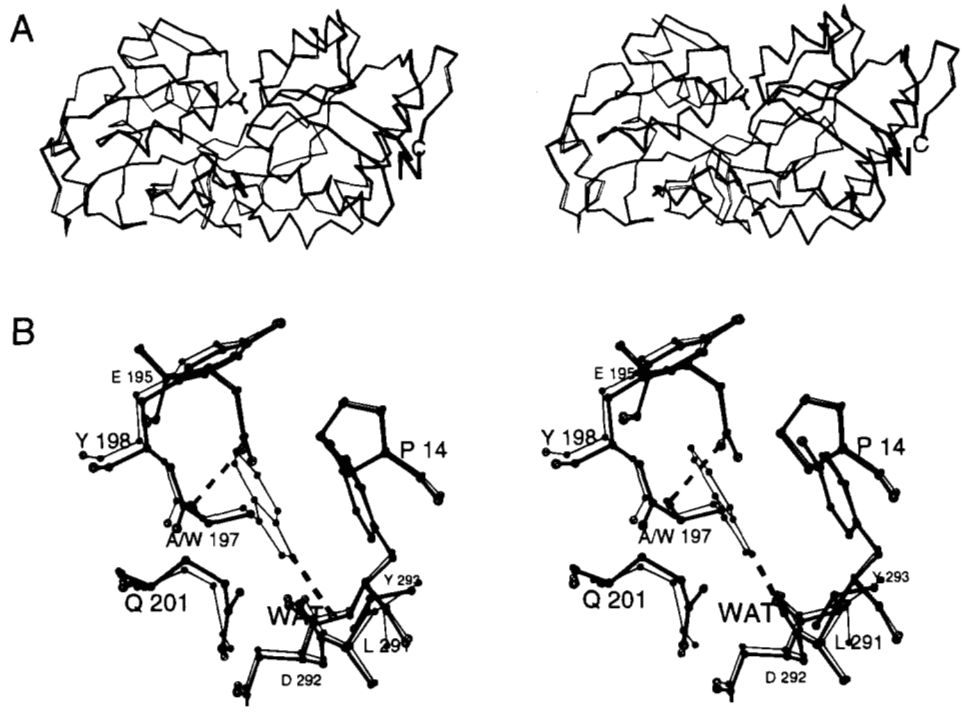

Fig. 5. A: α-Carbon backbone traces of both structures. Shown are the Trp197 replacement residue and the phosphate buried in the cleft between the two domains (Domain I on the right and Domain II on the left). **B:** A close-up view of Trp197 and nearby residues in Domain II. Residues Thr10 to Pro12, Pro14, and Leu291 to Tyr293 are located in Domain I. Orientation is identical to **A**.

hydrogen bond interactions of Ala197 with other residues in the wild-type structure are maintained in the mutant structure. One of these, between Ala/Trp197 N and Glu195 OE1, is shown in Figure 5B. The Trp replacement side chain is stabilized by surrounding residues, including Tyr198 and Gln201 in Domain II and Pro14, Leu291, and Tyr293 in Domain I, with their hydrophobic moieties in close contact with the Trp side chain.

Discussion

Perfect complementarity and stringent specificity between PBP and Pi are achieved mainly by means of hydrogen bonding or dipolar interactions (Fig. 6) (Luecke & Quiocho, 1990; Wang et al., 1997). The completely dehydrated and buried phosphate (in this case, a dibasic) is bound by 12 hydrogen bonds (distances from 2.432 to 2.866 Å, as determined from the 0.98 Å structure; Wang et al., 1997), equally distributed between the two domains, and by charge coupling with Arg135 that, in turn, is salt linked with Asp137 (Fig. 6). The PBP–Pi complex is formed even though the net formal charges of Pi (-2 for dibasic or -1 for monobasic) and the residues (-1) close to the Pi, as depicted in Figure 6, are negative. As phosphate binding activity occurs in a broad pH range (from 4.3 to 9), PBP binds both monobasic and dibasic phosphates (Luecke & Quiocho, 1990; Wang et al., 1994).

The presence of the uncompensated negatively charged carboxylate of Asp56 is the key to conferring the stringent specificity of PBP for phosphate over sulfate (Luecke & Quiocho, 1990; Ledvina et al., 1996). By making a hydrogen bond with Pi (Fig. 6), the carboxylate recognizes a proton on the phosphate. As the hydrogen bond is extremely short (2.432 Å), the hydrogen could be shared between the oxygens of the carboxylate and phosphate (Wang et al., 1997).

A related recent discovery is that Pi binding occurs in a binding cleft region with an intense negative electrostatic surface potential (Fig. 7) (Ledvina et al., 1996). This surface potential is believed to enhance phosphate specificity conferred by the dipolar interactions. The surface of the cleft confined to Domain I is entirely negative, partly due to contribution of Asp56 (Fig. 7B). The lone positive surface potential in the cleft in the midst of a wider negative surface in Domain II is from Arg135, which forms a salt link with Asp137 in the ligand-free and bound structures (Figs. 6, 7C) (Luecke & Quiocho, 1990; Ledvina et al., 1996; Yao et al., 1996).

Noncomplementarity between surface potential of a binding region and anion ligand is not unique to PBP. We have reported similar findings for a sulfate-binding protein, which is also a member of the large family of transport proteins to which PBP belongs, a DNA-binding protein, and, even more dramatically the redox protein, flavodoxin (Ledvina et al., 1996). In fact, the sulfate-binding protein and flavodoxin rely on hydrogen-bonding interactions with only uncharged residues for anion binding and electrostatic balance.

To further study the electrostatic effect on Pi binding, experiments were conducted under conditions of increasing ionic strength. Increased ionic strength might be expected to decrease charge repulsion between the incoming anion and the electronegative binding site surface, thus increasing the Pi binding affinity and reaction rate. In fact, no enhancement in binding affinity and rate due to increased shielding by solvent ions was observed. Rather, a decrease in affinity and rate was observed with increased ionic strength. This result indicates the greater importance of local, complemen-

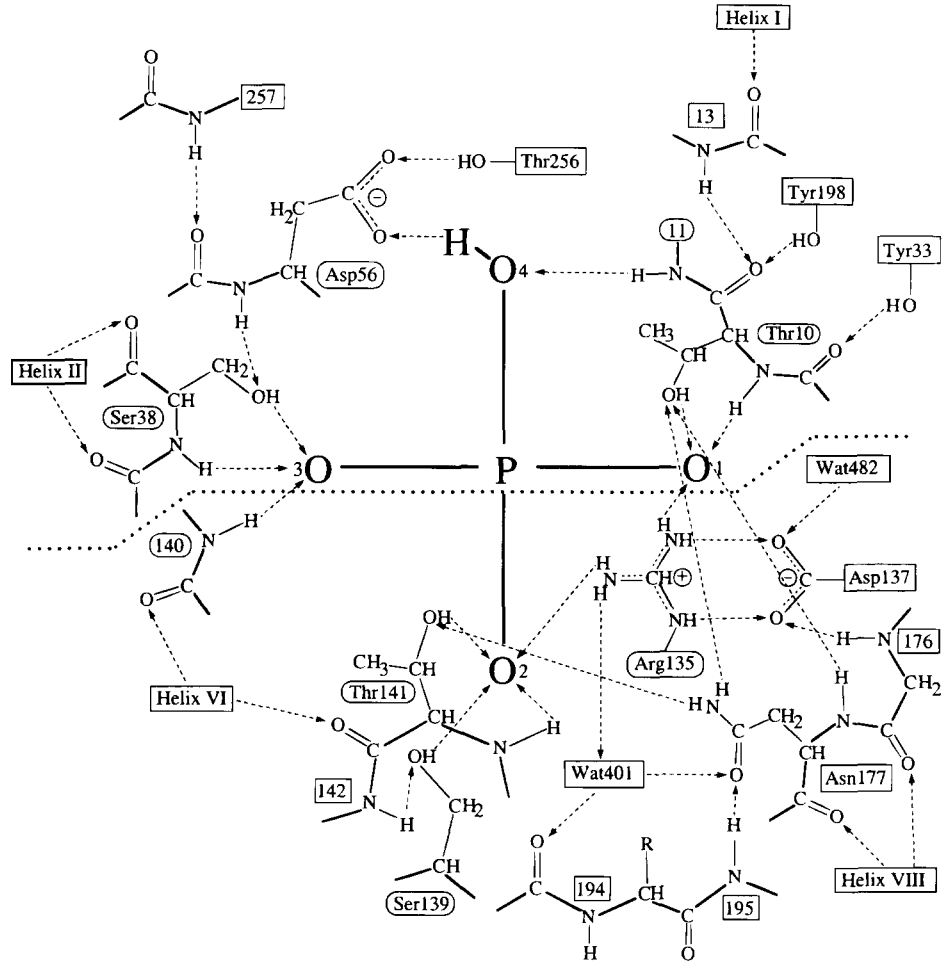

Fig. 6. Schematic diagram of the 12 hydrogen bonds between wild-type PBP and phosphate. The 12 hydrogen bonds (broken lines) have distances between 2.432 to 2.866 Å as determined from the 0.98 Å refined structure (Wang et al., 1997). The peptide backbone and side-chain groups (first shell) that make hydrogen bond with the Pi are further involved in hydrogen bond networks with other residues (second shell). Residues above the dotted lines (with the exception of Tyr198) reside in Domain I, whereas those below the dotted line belong to Domain II, in addition to Tyr198.

tary electrostatic interactions over long-range, potentially repulsive forces. This interpretation is consistent with experimental results showing that the specificity and affinity of the phosphate-binding protein for anions is insensitive to modulation of the surface charge potential of the cleft region, but extremely sensitive to electrostatic effects at the level of local hydrogen bonding interactions (Ledvina et al., 1996, and references therein).

With the understanding that the effect of ionic strength is localized to the direct interaction between PBP and Pi, what protein functional groups are likely involved? One set is represented by side chains with formal or full charges assuming normal pK_a, Asp56 with an uncompensated charge in Domain I, and Arg135 in Domain II (Figs. 6, 7B,C). Ion screening would be predicted to have opposing effects on these two charged residues. However, the apparent charge seen by HPO_4^{2-} (at pH 8.5) in the initial binding step could be partly due to Arg135. The Debye-Hückel theory predicts that a plot of $\log k_1/k_1^0$ (data from Table 3) vs. the square root of the ionic strength gives a line with a slope approximating the product of the charges of the PBP binding site (Z_{PBP}) and the ligand ($Z_{Pi} = -2$) (Nolte et al., 1980). Such an analysis yields an apparent Z_{PBP} of about +1.3. A problem with this interpretation is that Arg135 is salt linked with Asp137 (Figs. 6, 7B) in both the open and closed structures, and that modulations of this salt link do not affect the K_d of Pi binding. These modulations were effected by neutralizing Asp137 (Figs. 6, 7) or by substituting its negatively charged side chain with more electro-negative anions (e.g., bromide and chloride) through site-directed mutagenesis (Yao et al., 1996).

The other collection of groups consists of backbone NH and side-chain OH polar groups, with partial positive-charged proton donors to the phosphate (Fig. 6). The best experimental evidence for localized electrostatic shielding of partial charges of hydrogen bonding groups is the finding that increasing ionic strength also diminishes the sulfate-binding activity of the sulfate-binding protein (Pardee, 1966). The surface charge potential of the binding site of SBP, like that of PBP, is electronegative (Ledvina et al., 1996). Most significantly, crystallographic analysis shows that the sulfate, which is totally desolvated and sequestered in a cleft between two domains, is bound exclusively by hydrogen bonds with nonionizing polar groups (Pflugrath & Quiocho, 1985).

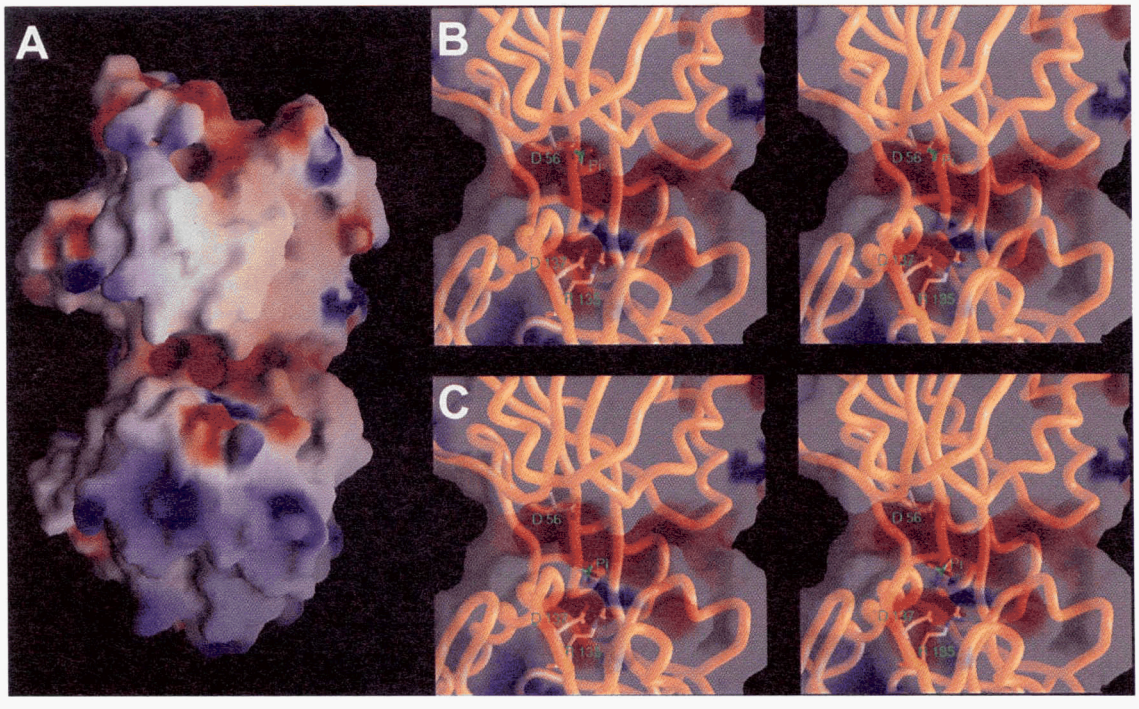

Fig. 7. Negative electrostatic surface potential of the cleft region that contains the phosphate-binding site of the native PBP in the open, ligand-free form. The molecular surface and electrostatic potential [-10 *kT* (red), neutral (white) and +10 *kT* (blue)] were calculated and displayed using GRASP (Nicholls et al., 1993). **A**: Entire wild-type PBP molecule with the cleft, in the middle of the molecule, separating the two domains (Domain I on top and Domain II on the bottom) (for details, see Ledvina et al., 1996). **B:** A close-up view (in identical orientation as in **A**) of the open cleft region rendered as a transparent surface with the polypeptide backbone trace shown in yellow color and the side chains of D56 from Domain I, D137 and R135 from Domain II included. There is no structure of the open form with bound Pi. The Pi (green stick model) has been modeled in Domain I of the open structure on the basis of its position with respect to the Asp56 residue as seen in the X-ray structures of the closed form of PBP with one molecule of bound Pi (Fig. 5; see also Luecke & Quiocho, 1990; Wang et al., 1994, Yao et al., 1996). In these X-ray structures, Pi makes a hydrogen bond with Asp56 (Fig. 6). **C:** Identical image as **A**, but with the Pi modeled in its position in Domain II, with respect to Arg135 residue of Domain II. Arg135 makes the same number of hydrogen bonds and salt link with Pi and Asp137 (Fig. 6).

It has been demonstrated by a variety of techniques, most clearly by X-ray crystallography, that isomerization of the binding proteins occurs as a hinge-bending motion between the two domains (for reviews, see Quiocho, 1991; Quiocho & Ledvina, 1996). The structures of the ligand-bound closed form have been determined for all (at least a dozen) binding proteins that have been subjected to X-ray analysis. Ligand-free open structures have been determined for some of these binding proteins, including PBP (Ledvina et al., 1996). There are X-ray structural data to indicate ligand binding to one domain in crystals of an open form of a binding protein (Sack et al., 1989). Very recently, we have determined the closed and open structures of the periplasmic maltodextrin-binding protein cocrystallized with oligosaccharides. Whereas the ligands are sequestered between the two domains in the closed form, they are bound exclusively to one domain in the open form (X. Duan et al., unpubl. obs.).

The kinetic studies described here offer the opportunity to assess the dynamics of the hinge-bending motion between the two domains of periplasmic binding proteins involved in active transport. The location of the mutation, by the mouth of the cleft and away from binding site, is compatible with the two-step ligand-binding mechanism we proposed. The Trp would be sensitive to the closure and not the initial phosphate binding to one domain. The study of hinged cleft motion in solution reported here is compatible with that on the periplasmic glucose/galactose-binding protein using disulfide trapping technique (Careaga et al., 1995).

The data, thus far, do not indicate with certainty which domain serve as an initial docking site for the ligand in the open form of PBP. Ligand binding to Domain I, which contains Asp56, would satisfy, in the initial binding step, the specificity requirement for the recognition of a phosphate hydrogen. On the other hand, the presence of Arg135 would seem to favor Domain II, a docking site that is potentially more susceptible to the changes observed with increasing ionic strength.

In conclusion, the results presented here provide further experimental evidence that complementarity of surface charges is not a prerequisite for high specificity and relatively tight ligand binding. Remarkably, in fact, the initial binding of phosphate is near diffusion-controlled rate. That the entire binding process depends almost entirely on local dipolar interactions between protein and anionic ligands has important ramification in electrostatic interactions in protein structures and in recognition of charged ligands or substrates in a variety of processes.

Materials and methods

Materials

Radioactive ^{32}Pi was purchased from Dupont/NEN. Oligonucleotides for mutagenesis or DNA sequencing were synthesized on an Applied Biosystems 380B DNA synthesizer.

Site-directed mutagenesis and expression of phoS (PBP)

Site-directed mutagenesis of the gene for PBP, *pho*S, was as previously described (Wang et al., 1994). The oligonucleotide, 5′-CTGCTTCGCGTA***CCA***ATATTCAACATAACC-3′, was used to replace the codon ***GCT*** (Ala) with ***TGG*** (Trp) at position 197. The mutated *phoS* was cloned into the *Nde*I/*Hind*III sites of Novagen pET-22b(+) to place it under control of bacteriophage T7 transcription and translation signals. For cloning, appropriate *Nde*I and *Hind*III sites were introduced to the coding region by PCR. The primer, 5′GCTATA***CATATG***AAAGTTATGCGTACC3′, was used to incorporate an *Nde*I site (bold italics) at the ATG start codon, and the primer 5′CGC***AAGCTT***ATTAGTACAGCGGCTTACC3′ was used to place a *Hind*III site (bold italics) just downstream from the TAA stop codon. High level expression of the recombinant, designated pET-PBP197W, was obtained using the host cell, BL21(D3), and a 4 h induction with IPTG (1 mM) at 37 °C in LB media.

Protein purification

Purification of the A197W PBP was as previously described for wild-type PBP (Kubena et al., 1986; Wang et al., 1994). Molar concentration of purified protein was determined from the absorbance at 280 nm using an extinction coefficient of 1.6 mg mL^{-1} cm^{-1} and a molecular weight of 34.4 kDa. To remove contaminating phosphate, 1 mL of protein (1–10 μM in H_2O) was equilibrated for 15 min with 0.4 mg of AG1X8 acetate resin and recovered by high-speed centrifugation.

Equilibrium binding assay

Phosphate-binding activity assays were measured by the resin method (Pardee, 1966; Medveczky & Rosenberg, 1970), which has been modified in our laboratory (Yao et al., 1996; Wang et al., 1997). The assays were conducted at room temperature using 0.1 g AG1X8 acetate resin, 42 μM ^{32}Pi (1.42×10^{13} CPM/mol), 3–5 μM protein, and 50 mM Tris-acetate, pH 8.5, in a 1.0-mL volume. Incubation mixtures were allowed to stand at room temperature for 15 min with intermittent mixing and then centrifuged for 2 min in a microfuge at 12 k rpm. Aliquots (80 μL) from the supernatant were counted for ^{32}Pi activity. Blank samples, containing no protein, were treated identically. The CPM value measured for the blank represents phosphate released from the resin, [Pi_{free}], which, under these conditions, is about 0.25 μM. The CPM value of the sample with protein represents both [Pi_{free}] and Pi bound by protein [Protein-Pi]. By subtracting [Pi_{free}] from this value, [Protein-Pi] is obtained. Finally, the concentration of unbound protein, [$Protein_{free}$], is obtained by subtracting [Protein-Pi] from the total protein. The K_d is then

$$\frac{[Pi_{free}] * [Protein_{free}]}{[Protein - Pi]}.$$

The average of three blanks is used in each experiment. Samples are run in triplicate to obtain the average K_d and standard deviation.

Following similar previous procedures (Miller et al., 1983; Vermersch et al., 1990), fluorescence titrations of the A197W PBP were conducted using an SLM/Aminco model 4800 spectrofluorometer with an excitation wavelength of 285 nm. Assays were conducted at 20 °C in 50 mM Tris-acetate, pH 8.5 and 0–900 mM NaCl. The fluorescence decrease at 330 nm was titrated by the addition of microliter aliquots of a concentrated Pi solution to 2 mL of protein. Under tight binding conditions (no NaCl added), titrations were conducted using a protein concentration of 0.09 μM. For other titrations (50–900 mM NaCl), the protein concentration was 1.0 μM. To correct for photo-oxidation, the fluorescence decrease at 330 nm was measured for an equivalent protein solution to which only buffer was added. For each addition of phosphate or buffer, an average of 10 measurements were recorded. Titrations in conditions of 0–100 mM NaCl were conducted in duplicate. Binding data for high salt conditions (300, 600, and 900 mM) were obtained from single titrations at each concentration. Prior to use, cuvettes were incubated with a "Pi mop" (1 mM 7-methylguanosine and 1 unit/mL purine nucleoside phosphorylase in 10 mM PIPES, 1 mM $MgCl_2$, pH 7.0) to remove contaminating phosphate (Brune et al., 1994).

Ligand-binding kinetics

The transient kinetic measurements of the reaction between A197W PBP and Pi were done in a Bio-Sequential DX-18MV stopped-flow apparatus (Applied Photophysics, Leatherhead, UK). The dead time of mixing was approximately 1.5 ms. The excitation wavelength was 285 nm, with 2-mm slits, and emission was followed at wavelengths >325 nm. Experiments were performed at 25–27 °C in 50 mM Tris-acetate, pH 8.5, and 0–900 mM NaCl, as indicated. For each Pi concentration, 5–10 repeat shots were performed. Association rates were measured using 1.0 μM protein and [Pi] in the range of 1–200 μM and fit to a single exponential function. Prior to each use, the stopped-flow apparatus was incubated with the Pi mop to remove residual phosphate. The Simulation Control Program (SCoP) from Simulation Resources, Inc., Berrien Springs, Michigan, was used for data fitting and simulations.

X-ray structure determination

Crystals of the A197W PBP in the presence of Pi were obtained by using a procedure similar to that for the wild-type PBP complexed with phosphate (Kubena et al., 1986; Luecke & Quiocho, 1990). One large crystal was grown from a seed at room temperature in a 4-μL droplet containing 5.5 mg/mL protein, 1.5 mM potassium phosphate, 15.0% (w/v) polyethylene glycol 6000, 37.5 mM KCl, 15 mM potassium acetate, pH 4.5, hanging over a well solution of 1 mL 20% (w/v) polyethylene glycol 6000, 50 mM KCl, 2 mM potassium phosphate, and 20 mM potassium acetate, pH 4.5. The crystal was harvested in a well solution containing 22% polyethylene glycol 6000. Prior to data collection the crystal was progressively transferred to the same solution containing increasing amounts of glycerol cryoprotectant (5, 10, 15, 20, and 25%) and then flash cooled to −170 °C with a cryogenic cooling unit.

Diffraction data were collected using a MAC Science DIP2030 image plate system with double-mirror focusing optics mounted on a Rigaku RU-200 rotating anode (CuK_α) operated at 50 kV and 90 mA. The data were processed and merged by DENZO and SCALEPACK (Otwinowski & Minor, 1997). The space group and unit cell dimensions are essentially identical to those of the wild-type crystals (Table 3) (Kubena et al., 1986; Luecke & Quiocho, 1990).

The XPLOR program Version 3.85 (Brünger, 1992), with the parameters of Engh and Huber (Engh & Huber, 1991), was used in the refinement of the A197W PBP structure. The CHAIN program

(Sack & Quiocho, 1997) was used in fitting the model to the electron density maps and examination of the structures. As the mutant crystals are isomorphous with the native crystals, the initial model used for the refinement was the 1.66 Å resolution structure of the native liganded form of PBP refined by XPLOR (Wang et al., 1994) (Table 3), with the exclusion of water molecules and no modeling of the Trp197. After one cycle of rigid-body refinement, the *R*-factor dropped to 25%. Positional refinement followed by *B*-factor refinement was conducted several times and interspersed with examination of $(2|F_o| - |F_c|, (\alpha_c)$ and $(|F_o| - |F_c|, \alpha_c)$ maps to improve, when necessary, the fit of the model to density and to locate water molecules. Following further cycle of refinement, the Trp197 side chain and phosphate could be easily fitted to both types of electron density maps. Diffraction data and final refinement statistics are shown in Table 3. Note that in the refinement of the A197W and native PBPs, the unique reflections after merging with no sigma cutoff (36,946 and 35,260 reflections, respectively) were used. Coordinates of the A197W PBP structure have been deposited in the Brookhaven Protein Data Bank (1A40).

Acknowledgments

We thank Dr. J.S. Olson for helpful discussion and W. N. Meador for technical assistance. This work has been supported in part by grants from NIH (GM-44911) to A.-L.T., NIH (GM-21371) and Welch Foundation (Q-0581) to F.A.Q., and NSF (STI-9512521) to the Biomedical Computation and Visualization Laboratory, Baylor College of Medicine. F.A.Q is an Investigator in the Howard Hughes Medical Institute.

References

Åqvist J, Luecke J, Quiocho FA. 1991. Dipoles localized at helix termini of proteins stabilize charges. *Proc Natl Acad Sci USA 88*:2026–2030.

Brune M, Hunter JL, Corrie JE, Webb MR. 1994. Direct, real-time measurement of rapid inorganic phosphate release using a novel fluorescent probe and its application to actomyosin subfragment 1 ATPase. *Biochemistry 33*:8262–8271.

Brünger AT. 1992. *X-PLOR, Version 3.1, A system for X-ray crystallography and NMR*. New Haven, Connecticut: Yale University.

Careaga CL, Sutherland J, Sabeti J, Falke JJ. 1995. Large amplitude twisting motions of an interdomain hinge: A disulfide trapping study of the galactose–glucose binding protein. *Biochemistry 34*:3048–3055.

Cleland WW, Kreevoy MM. 1994. Low-barrier hydrogen bonds and enzymic catalysis. *Science 264*:1887–1890.

Engh RA, Huber R. 1991. Accurate bond and angle parameters for X-ray protein structure refinement. *Acta Crystallogr A47*:392–400.

He JJ, Quiocho FA. 1993. Dominant role of local dipoles in stabilizing uncompensated charges on a sulfate sequestered in a periplasmic active transport protein. *Protein Sci 2*:1643–1647.

Hibbert F, Emsley J. 1990. Hydrogen bonding and chemical reactivity. *Adv Phys Org Chem 26*:255–379.

Jacobson BL, He JJ, Lemon DD, Quiocho FA. 1992. Interdomain salt bridges modulate ligand-induced domain motion of the sulfate receptor protein for active transport. *J Mol Biol 223*:27–30.

Kang CH, Shin WC, Yamagata Y, Gokcen S, Ames GF, Kim SH. 1991. Crystal structure of the lysine-, arginine-, ornithine-binding protein (LAO) from *Salmonella typhimurium* at 2.7 Å resolution. *J Biol Chem 266*:23893–23899.

Kubena BD, Luecke H, Rosenberg H, Quiocho FA. 1986. Crystallization and x-ray diffraction studies of a phosphate-binding protein involved in active transport in *Escherichia coli*. *J Biol Chem 261*:7995–7996.

Ledvina PS, Yao N, Choudhary A, Quiocho FA. 1996. Negative electrostatic surface potential of protein sites specific for anionic ligands. *Proc Natl Acad Sci USA 93*:6786–6791.

Luecke H, Quiocho FA. 1990. High specificity of a phosphate transport protein determined by hydrogen bonds. *Nature 347*:402–406.

Medveczky N, Rosenberg H. 1970. The phosphate-binding protein of *Escherichia coli*. *Biochim Biophys Acta 211*:158–168.

Miller DM III, Olson JS, Pflugrath JW, Quiocho FA. 1983. Rates of ligand binding to periplasmic proteins involved in bacterial transport and chemotaxis. *J Biol Chem 258*:13665–13672.

Miller DM III, Olson JS, Quiocho FA. 1980. The mechanism of sugar binding to the periplasmic receptor for galactose chemotaxis and transport in *Escherichia coli*. *J Biol Chem 255*:2465–2471.

Nicholls A, Bharadwaj R, Honig B. 1993. Grasp: Graphical representation and analysis of surface properties. *Biophys J 64*:166–170.

Nickitenko AV, Trakhanov S, Quiocho FA. 1995. 2 Å resolution structure of DppA, a periplasmic dipeptide transport/chemosensory receptor. *Biochemistry* 34:16585–16595.

Nolte HJ, Rosenberry, TL, Neumann E. 1980. Effective charge on acetylcholinesterase active sites determined from the ionic strength dependence of association rate constants with cationic ligands. *Biochemistry 19*:3705–3711.

Otwinowski Z, Minor W. 1997. Processing of X-ray diffraction data collected in oscillation mode. *Methods Enzymol 276*:307–326.

Pardee AB. 1966. Purification and properties of a sulfate-binding protein from *Salmonella typhimurium*. *J Biol Chem 241*:5886–5892.

Pflugrath JW, Quiocho FA. 1985. Sulphate sequestered in the sulfate-binding protein is bound solely by hydrogen bonds. *Nature 314*:257–260.

Quiocho FA. 1991. Atomic structure and function of periplasmic receptors for active transport and chemotaxis. *Curr Opin Struct Biol 1*:922–933.

Quiocho FA, Gilliland GL, Phillips GN Jr. 1977. The 2.8-Å resolution structure of the L-arabinose-binding protein from *Escherichia coli*. Polypeptide chain folding, domain similarity, and probable location of sugar-binding site. *J Biol Chem 252*:5142–5149.

Quiocho FA, Ledvina PS. 1996. Atomic structure and specificity of bacterial periplasmic receptors for active transport and chemotaxis: Variation of common themes. *Mol Microbiol 20*:17–25.

Quiocho FA, Sack JS, Vyas NK. 1987. Stabilization of charges on isolated charged groups sequestered in proteins by polarized peptide units. *Nature 327*:561–564.

Sack JS, Quiocho FA. 1997. CHAIN—A crystallographic modeling program. *Methods Enzymol 277*:158–173.

Sack JS, Saper MA, Quiocho FA. 1989. Periplasmic binding protein structure and function. Refined X-ray structures of the leucine/isoleucine/valine-binding protein and its complex with leucine. *J Mol Biol 206*:171–191.

Vermersch PS, Tesmer JJ, Lemon DD, Quiocho FA. 1990. A Pro to Gly mutation in the hinge of the arabinose-binding protein enhances binding and alters specificity. Sugar-binding and crystallographic studies. *J Biol Chem 265*: 16592–16603.

Walmsley AR, Shaw JG, Kelly DJ. 1992. The mechanism of ligand binding to the periplasmic C4-dicarboxylate binding protein (DctP) from *Rhodobacter capsulatus*. *J Biol Chem 267*:8064–8072.

Wang Z, Choudhary A, Ledvina PS, Quiocho FA. 1994. Fine tuning the specificity of the periplasmic phosphate receptor for active transport. Site-directed mutagenesis, ligand binding, and crystallographic studies. *J Biol Chem 269*:25091–25094.

Wang Z, Luecke H, Yao N, Quiocho FA. 1997. A low energy short hydrogen bond in very high resolution structures of protein receptor–phosphate complexes. *Nat Struct Biol 4*:519–522.

Yao N, Ledvina PS, Choudhary A, Quiocho FA. 1996. Modulation of a salt link does not affect binding of phosphate to its specific active transport receptor. *Biochemistry 35*:2079–2085.

Yao N, Trakhanov S, Quiocho FA. 1994. Refined 1.89-Å structure of the histidine-binding protein complexed with histidine and its relationship with many other active transport/chemosensory proteins. *Biochemistry 33*:4769–4779.